IEEE Access
Multidisciplinary | Rapid Review | Open Access Journal

Received March 17, 2017, accepted April 20, 2017, date of publication April 26, 2017, date of current version June 7, 2017.

Digital Object Identifier 10.1109/ACCESS.2017.2698061

A Magnetic Induction-Based Highly Dynamic Rotational Angular Rate Measurement Method

KAI LI[1], (Member, IEEE), YUAN LI[2], AND YAN HAN[3]

[1]Department of the Shanxi Key Laboratory of Signal Capturing and Processing, North University of China, Taiyuan 030051, China
[2]School of Information and Communication Engineering, North University of China, Taiyuan 030051, China
[3]Department of the National Key Laboratory for Electronic Measurement Technology, North University of China, Taiyuan 030051, China

Corresponding author: Kai Li (likai@nuc.edu.cn)

This work was supported in part by the National Natural Science Foundation of China under Grant 61227003 and in part by the National Basic Research Program of China (973 Program) under Grant 2013CB311804.

ABSTRACT A magnetic induction-based angular rate measurement method is proposed to address the need for internal measurement of high-speed angular rate of carriers. This method relies on the rotational periodicity fed back by the magnetic field. Three coils aligned orthogonal one to another are employed as the feedback module that supplies the rotational periodicity information, the physical characteristic that contains the periodic signals, which in turn reflect the highly dynamic rotation of the carrier in its accelerating process. The periodic, instantaneous start point is extracted from the magnetic signal using zero-phase threshold technique, whereby the signal periodicity is established, enabling experimental measurement of the rotational angular rate of a high-speed rotation object. A semi-physical simulation was conducted at different speeds using a low maximum speed high-precision rotary table, and the results demonstrate that this measurement method is capable of measuring angular rate varying dynamically between 1 and 100 r/s, with a measurement error within 2‰ of the full scale. This method also provides a means for evaluating angular rate of other types of rotational movement.

INDEX TERMS Electromagnetic induction, rotation measurement, angular velocity, high dynamic rotation, high rotational speed, zero-phase detection.

I. INTRODUCTION

Ever increasing needs arise for measuring carrier parameters in modern industries, civil and military applications where accurate control of rotational carrier is desired. This situation creates an important research direction: highly dynamic angular rate measurement of carriers. By use of hi-speed rotation, a carrier may get rid of flight path variation caused by propulsion eccentricity, mass eccentricity, or aerodynamic eccentricity [1]–[3]. A carrier stabilized by hi-speed rotation offers such benefits as simple internal construction, low control cost, and low energy consumption, but the hi-speed rotation tends to give rise to error accumulation in the internal measurement elements [4]–[6]. The measurement elements shall come with a wide rotation adaptability in order to secure steady and hi-precision angular rates, but this makes the elements unable to satisfy at the same time the measurement accuracy requirement at low- and high-speed rotation [7], [8]. A higher element sensitivity contributes, on the one hand, to higher measurement accuracy at low rotation speeds, but drives up the accumulated error of the element at high rotation speeds, resulting in unsteady measurement accuracy and, thus, degrading carrier control performance [8]. Highly dynamic carrier angular rate measurement has therefore become one research hot spot in this field over recent years [9]. Using a wide range angular rate measurement element to acquire highly dynamic angular rate of a rotational carrier are beneficial on multiple fronts. It not only helps accurately obtain highly dynamic rotational movement parameters, which improves the control of the hi-speed rotational carrier flight path and guides carrier structure optimization, but also provides design basis for the benefit of carriers that rely on hi-speed rotation for stability.

The angular rate of highly dynamic rotational carriers is typically measured using an external auxiliary means or an internal element. External auxiliary method relies on external auxiliary equipment to measure directly the physical feedback information of the measured object in its movement process and evaluates the angular rate based on the

periodicity of physical characteristics [10], [11]. External auxiliary equipment, such as a tachometer, is installed at a specified location, capable of capturing hi-precision angular rate of hi-speed rotational objects [12], [13], but it is unable to track the entire flight path of the object. This method comes therefore with limitation when used to measure angular rate of carriers. In contrast, internal measurement methods use elements with different physical characteristics to directly measure the angular rate of the object in the course of flight, capable of providing an all-path measurement solution. Typically reported in researches on internal element measurement methods are those making use of inertial element [14], [15], optical element [16], magnetic sensor [17], [18], or GPS module [19]. Extracting inertial parameters by means of inertial element is effective in capturing mechanical characteristics and dynamics feedback of the carrier at a low-speed rotation or when interaxial interference is absent, and in the gravity field this type of methods provide well-proven measurement models and wide applicability [20]. Optical elements enable capturing star light information in the ambience in which the carrier exists. From star light azimuth and the periodicity of the light hitting the carrier, it is possible to deduce under certain time and weather conditions the angular rate of the carrier [21], [22]. A magnetic sensor provides magnetic field information of the ambience in which the carrier flies and, in the absence of magnetic material interference, the angular rate of the carrier may be evaluated by solving for magnetic field vectors [23], [24]. Multiple GPS modules are installed on the carrier and its angular rate is estimated by manipulating the data of these hi-precision GPS modules. This type of methods work in places with GPS coverage and free from GPS interference and may provide hi-precision estimation of angular rate at low-speed rotation [24]. On the whole, existing literature on angular rate measurement focuses for the most part on hi-precision measurement of low-speed rotation or hi-precision stationary measurement of angular rate. There is no any reported research that investigates measuring the angular rate of hi-speed rotation carriers in a highly dynamic movement process.

This paper presents a magnetic induction method for measuring highly dynamic angular rate. This method works by processing magnetic field information fed back during the highly dynamic rotational movement of the carrier. Three magnetic induction coils aligned orthogonal one to another acquire, on a real-time basis, the periodic signal fed back by the magnetic field in the dynamic acceleration process. The periodicity of rotational movement is evaluated using zero-phase signal threshold processing technique, and a variation curve is constructed that incorporates angular rate of rotational movement. The carrier's angular rate is then estimated using a signal filtering algorithm. The measurement in a highly dynamic variation process of angular rate was compared to the setting of a hi-precision rotary table and it was found that the angular rate measurement error is within 2‰ of the full scale (FS), validating the proposed method.

Using magnetic signal threshold zero-phase detection technique, the proposed measurement method provides immunity to influence caused by magnetic material and enables the carrier to provide periodic vector feedback on the magnetic field information, and therefore accomplishes all-path, highly dynamic, and high rotation speed angular rate measurement.

This paper presents a magnetic induction method for measuring highly dynamic angular rates. This method works by processing magnetic field information fed back during the highly dynamic rotational movement of the carrier. Three magnetic induction coils aligned orthogonal one to another acquire, on a real-time basis, the periodic signal fed back by the magnetic field in the dynamic acceleration process. The periodicity of rotational movement is evaluated using zero-phase signal threshold processing technique, and a variation curve is constructed that incorporates angular rate of rotational movement. The carrier's angular rate is then estimated using a signal filtering algorithm.

II. A MEASUREMENT SYSTEM OF HIGHLY DYNAMIC ANGULAR RATES

To define in a coordinate system the rotational movement of the carrier, we set the carrier center of gravity at the origin o, take the vertical direction pointing upward, when in the initial position, as axis z, the carrier axis as axis x, and the line passing through the origin and perpendicular to axes x and z as axis y, with the x, y, z constituting a right-hand rule coordinate system. In its rotational movement, the carrier performs a motion described by Euler kinematical equations. A set of triaxially orthogonal magnetic induction oils are installed in the carrier, as shown in Fig. 1, in order to measure its angular rate.

The set of triaxially orthogonal coils installed in the carrier rotate with it. As they are rotating in a magnetic environment, induction currents are created on the coils, which in turn create electromotive forces (EMFs). The induced EMFs are acquired as the signal fed back by the carrier in rotation. When acquired, the signal is conditioned to remove noises and then the signal phases are measured. Phase analysis helps us determine the periodicity of the induction signal, and this periodicity reflects the carrier's rotational period.

III. LAYOUT OF TRIAXIALLY ORTHOGONAL MAGNETIC INDUCTION COILS

To acquire the magnetic field feedback on the carrier, three magnetic coils are installed orthogonal one to another (Fig. 2) so as to sense the carrier's cutting the geomagnetic field in the rotational movement.

The centerline of coils X_c, Y_c, and Z_c points respectively to the positive direction of x, y, and z axes of the carrier's coordinate system. The coordinate origin is set on the flying body center of mass, with the three coil sensitive axes in parallel with the three axes of the carrier's coordinate system. The sensitive axes are placed, in theory, parallel with the coordinate axes such that the signal components

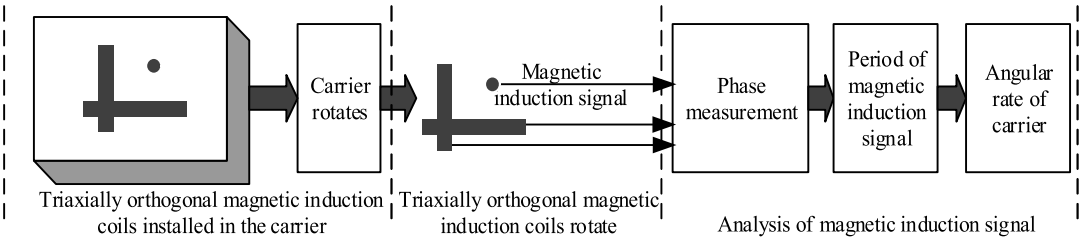

FIGURE 1. Implementation process flow of measurement of highly dynamic angular rates.

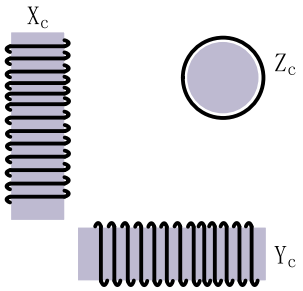

FIGURE 2. Layout of magnetic induction coils.

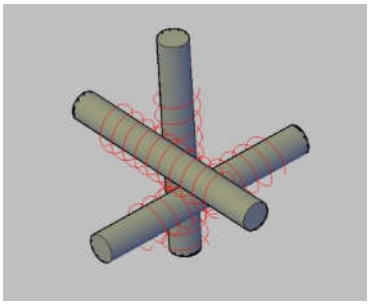

FIGURE 3. A 3D view of the layout of magnetic induction coils.

in the carrier's axial directions are measured to the highest accuracy, but in practice some installation errors are unavoidable. A premium is put on miniaturized and hi-sensitivity sensors, but too many turns would give rise to noticeable magnetic leakage, greater noise, and lower SNRs, so a proper number of turns is desirable. Moreover, as the carrier cannot be solely made up of non-ferromagnetic materials, the magnetic field information picked up by the coils would be the sum of the geomagnetic field, the magnetic field created by the carrier's magnetic materials, and the external interference magnetic field. In recognition of the above, the following assumptions are made: first, the installation error is neglected in theoretical analysis; second, ferromagnetic materials only affect the field within the carrier, and only create a stable and weak magnetic field, the impact on the distribution of the coil induction field being neglected; third, the carrier is homogeneous and axially symmetrical both in shape and mass, and there is no dramatic change in the flight path.

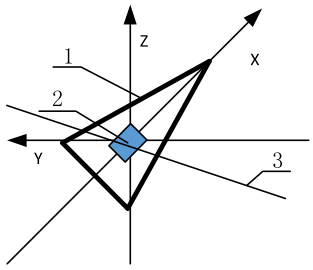

FIGURE 4. Diagram of the magnetic induction module as installed on the carrier.

IV. MAGNETIC FIELD RESPONSE OF THE TRIAXIALLY ORTHOGONAL MAGNETIC INDUCTION COILS WHEN THE CARRIER ROTATES

When an object rotates, as shown in Fig. 4, the instantaneous magnetic field vector remains unchanged, with the triaxially orthogonal coils rotating along with the object. In a complete rotation period, the coils coincide with the magnetic vector direction twice, and the coils generate a sinusoidal signal. Faraday's law of electromagnetic law and the magnetic physics knowledge tell us the magnetic flux variation within a closed coil that cuts a magnetic field will give rise to the following induced electromotive force (EMF):

$$E = \frac{d\phi}{dt} = NBS \sin \omega t \tag{1}$$

where, N is the number of turns, B the magnetic field strength responsible for coil induction, S the area enclosed by the coil, and ω the angular speed at which the coil rotates.

As can be concluded from the above equation, the triaxially orthogonal magnetic induction coils have a maximum EMF of:

$$E = NBS\omega \tag{2}$$

We may consider the output of the coils: B is the ambience magnetic field in which the carrier is situated, and the coil area S and the number of turns N are constants in the course of measurement. The induced EMF output by the coils is therefore dictated by ω, the rotational angular rate of the carrier.

We now consider the induced EMF output by coil X_c. The original carrier coordinate system coincides with the

geographic coordinate system, the carrier has in it a magnetic induction strength of B, whose components are B_{gx}, B_{gy}, B_{gz} in the geographic coordinate system or B_x, B_y, B_z in the carrier coordinate system, a magnetic declination of D, and a magnetic inclination of I. Then, in the geographic coordinate system the geomagnetic strength may be written as:

$$\begin{bmatrix} B_{gx} \\ B_{gy} \\ B_{gz} \end{bmatrix} = \begin{bmatrix} -B\sin D \\ B(\cos D + \cos I) \\ -B\sin I \end{bmatrix} \tag{3}$$

The three coils having identical effective area S as well as number of turns N, according to Faraday's law of electromagnetic induction the magnetic flux of coil A is give by:

$$\phi_C = \int_{SC} \vec{B} \cdot d\vec{S}_C = NBS\sin\omega t \tag{4}$$

When coil X_c rotates at an angular speed of ω about axis X of the carrier coordinate system: B_x is normal to coil X_c, hence the magnetic flux of coil X_c remains constant, with no induction EMF generated, however this coil generates EMF if it is not installed to coincide with the carrier's coordinate axis or if the carrier wobbles while rotating; coils Y_c and Z_c rotate about axis X, thus in parallel with plane YOZ, and B_y, B_z do not penetrate coil X_c but penetrate coils Y_c and Z_c, so magnetic flux running through these two coils varies. If coils X_c, Y_c, and Z_c in the initial state are parallel with the carrier coordinate x, y, and z axes, the magnetic flux ϕ_{Cx}, ϕ_{Cy}, and ϕ_{Cz} through the three coils would be:

$$\begin{cases} \phi_{Cx} = aNSB_{yz}\sin(\omega t + \Delta\omega_x) \\ \phi_{Cy} = NSB_{yz}\sin(\omega t + \Delta\omega) \\ \phi_{Cz} = NSB_{yz}\sin(\omega t + \Delta\omega + \pi/2) \end{cases} \tag{5}$$

where, a is a proportionality coefficient, reflecting coil X_c's feedback on the magnetic field while the coil rotates because the coil centerline is not installed to coincide with axis x of the carrier coordinate; $B_{yz}$is a function of B_y and B_z, with $B_{yz} = \sqrt{B_y^2 + B_z^2}$; $\Delta\omega_x$ is the included angle between X_c's projection on plane YOZ and the vector magnetic field direction; and $\Delta\omega$ is the spatial included angle between Y_c and the vector magnetic field direction.

When the carrier in the flight course rotates about the carrier coordinate axis y or z, the movement magnitude is small and the rotational movement of the two axes change little, so such movements are neglected in evaluating the rotational angular rate of the carrier.

Therefore, when triaxially orthogonal coils rotate about axis x, the induced EMF of the three coils are given by:

$$\begin{cases} E_{Cx} = -\dfrac{d\phi_{Cx}}{dt} = aNSB_{yz}\cos(\omega t + \Delta\omega_x) \\ E_{Cy} = -\dfrac{d\phi_{Cy}}{dt} = NSB_{yz}\cos(\omega t + \Delta\omega) \\ E_{Cz} = -\dfrac{d\phi_{Cz}}{dt} = NSB_{yz}\cos(\omega t + \Delta\omega + \pi/2) \end{cases} \tag{6}$$

Eq. (6) constitutes the magnetic response formulae of triaxially orthogonal coils rotating about a sole axis and contains the angular rate information of the three carrier axes.

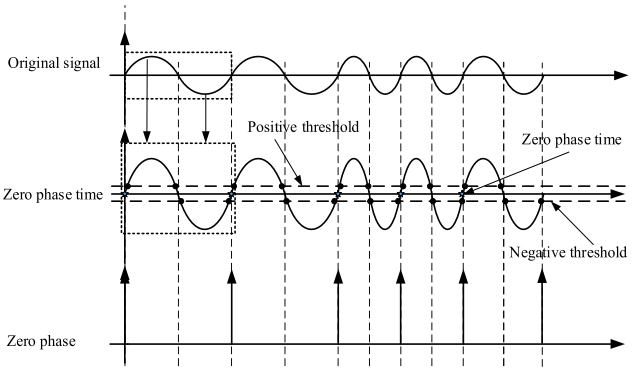

FIGURE 5. Conversion process of coil sensor zero phase signal.

FIGURE 6. Layout of triaxially orthogonal coils in a hi-precision rotary table.

V. ANALYSIS OF MAGNETIC INDUCTION SIGNAL

The phase of the measured signal is a response to the variation celerity, the periodicity, the rotational effect, the impact effect, and the vibration effect of physical quantities. Major techniques for finding the initial start point of the phase include rising and trailing signal edge analysis and processing as well as time and space conversion. Then, phase measurement of the signal is attained by analyzing phase details using phase grouping or time-space conversion in combination [25], [26].

This study relies on triaxially orthogonal magnetic induction coils to determine the carrier rotational angular rate. The inducted EMF output by the coils are sinusoid-like signal, whose period reflects the carrier's rotational angular rate.

The EMF signal contains noises of various frequencies, and so primary filtering is needed to reduce high frequency interferences in the physical environment and to improve the SNR. The EMF signal strength after primary filtering is weak, on the order of mV, so signal amplification becomes necessary. The signal, when amplified, goes through secondary filtering, whereby the amplified signal is processed by a low-pass filter such that the low-frequency signal is retained and jitter noise is removed.

As illustrated in Fig. 5, the original signal is the induced EMF output by the three coils. The signal is then studied in threshold analysis, which involves comparison against

positive or negative threshold. Signal greater than ''zero'' is compared against the positive threshold, signal below ''zero'' is compared against the negative threshold, and signal falling between positive and negative thresholds is deemed to be noise. What comes next is solving for zero phase. A zero phase is believed to exist when the signal crosses the negative and the positive thresholds consecutively, and the midpoint between the two thresholds is taken to be the zero phase point. A zero phase is believed to terminate when the signal crosses the negative and the positive thresholds consecutively, with the midpoint between the two thresholds regarded as the zero phase endpoint. The zero-phase point in the periodic signal is the start of the period and the zero-phase endpoint is the end of the periodic signal. A period starts at the zero-phase point and ends at the zero-phase endpoint.

Once the angular rate measurement begins, the first zero-phase point is taken as the start point t_0 of the initial and first period, and the second one serves as the start point t_1 of a steady period, symbolizing the begin of zero phase counter, and each subsequent zero-crossing point t_i then acts as the half-period time of the sensor signal.

Signal periodicity is determined based on zero-phase point information. With the signal varying at this frequency, the periodic variation times of this signal may be found by means of threshold analysis, from which the angular rate of the rotational body is deduced:

$$\omega = (t_{i+1} - t_i)/2 \tag{7}$$

Where, i is 0, 1, 2, 3 . . .

VI. EXPERIMENTAL RESULTS AND DISCUSSION

Multiple layers of wound coils were used in the test. The coil area was $1cm^2$, the wire diameter was 0.09mm, the number of turns was 9500, and the coil resistance was 665Ù. Given that the local geomagnetic strength is $0.5E - 4T$, it then follows that at a rotation speed up to 100rps(revolutions per second) the maximum EMF is $0.005mV$. But in practical applications the rotational speed can vary in a wide range and, in applications with a small rotational speed range, it is advisable to increase the number of turns as appropriate and to complete signal amplification and gain adjustment in the magnetic signal conditioning circuit, otherwise induced EMF with low SNR will be generated.

A. LOW ROTATIONAL SPEED SIMULATION

The simulation was performed using a hi-precision rotary table, where the triaxially orthogonal coils were attached to a stationary plane on the table. Coil Y_c, placed 40mm off from the table center axis, rotated when the table began to rotate at a constant acceleration. The rotational speed was kept constant for a while when it had accelerated to 1 rps, then the rotation was decelerated at a constant rate until coming to a stop. The sensor output voltage values, as measured in the course of rotation, were used to provide the solution, and the results were compared with the preset rotation speed of the table to determine the sensor angular rate accuracy.

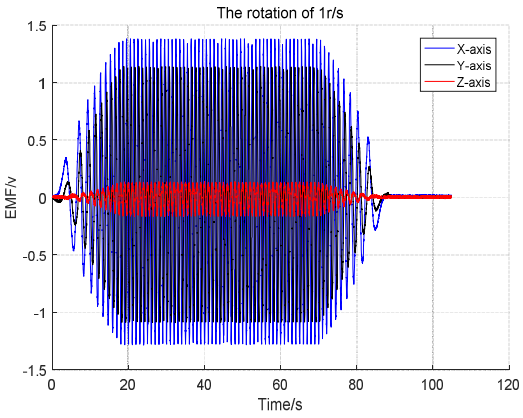

FIGURE 7. Sensor's induced voltage when the rotary table intermediate coil rotation rate is 1rps.

The table was accelerated to 360°/s at a constant acceleration of $20°/s^2$. The induced EMF output by the triaxially orthogonal coils is shown in Fig. 7, where the output voltages of axes X and Z are a function of ω, nevertheless axis Y would output induced EMF because coil Y_c was installed with eccentricity.

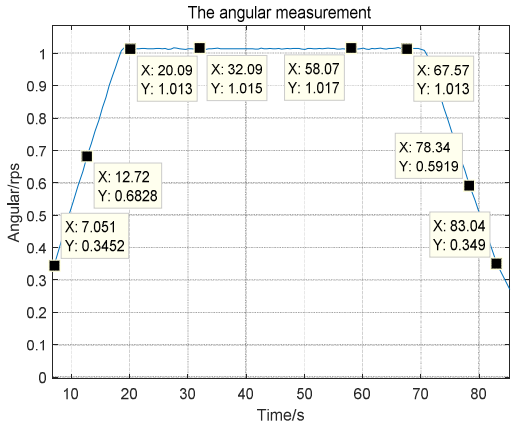

FIGURE 8. Instantaneous intermediate coil angular speed output by magnetic sensor electronic solver module.

As is known from Fig. 8, the triaxially orthogonal coils read an angular rate of 1.013-1.018rps when the rotary table stabilized at 1rps, producing an error of 0.13-0.18%FS; the initial angular rate measurement error was greater, which can be explained by the unstable measurement of zero-crossing signal at initial stage.

B. MEDIUM ROTATIONAL SPEED SIMULATION

The table was accelerated to 40r/s at a constant acceleration of $20°/s^2$. The induced EMF output by the triaxially orthogonal coils is shown in Fig. 9, where the output voltages of axes X and Z are a function of ω, nevertheless axis Y would output induced EMF because coil Y_c was installed with eccentricity.

As is apparent from Fig. 10, the triaxially orthogonal coils read an angular rate of 40.03-40.07rps when the rotary table

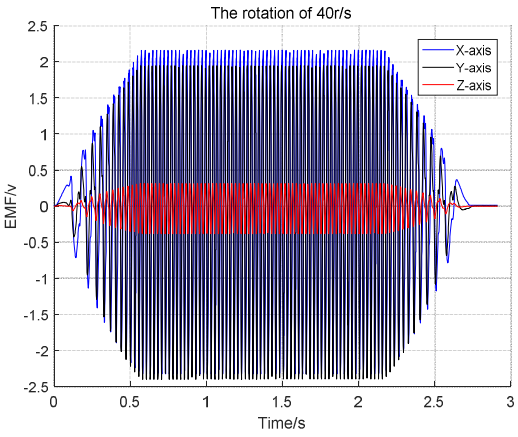

FIGURE 9. Instantaneous intermediate coil angular speed output by magnetic sensor electronic solver module.

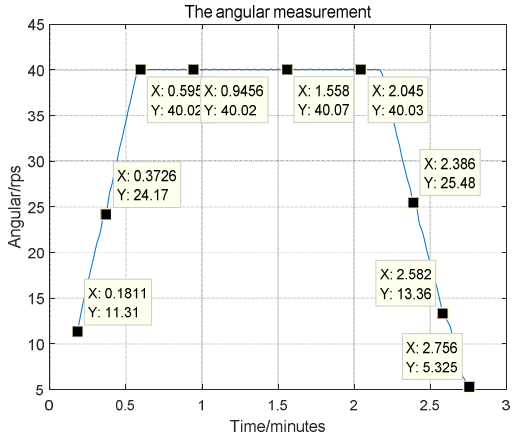

FIGURE 10. Instantaneous intermediate coil angular speed output by magnetic sensor electronic solver module.

stabilized at 1rps, producing an error of 0.075-0.175%FS; the initial angular rate measurement error was greater, which is explained by the unstable measurement of zero-crossing signal at initial stage.

C. HIGH ROTATIONAL SPEED SIMULATION

The sensor was mounted on a single-axle high-speed rotary table, which was started with a set angular speed of 100rps. The table cannot be accelerated to its set value in one step, so this was done in three steps. At the end of each acceleration (to 83r/s, 90r/s, and 100r/s respectively), the machine was allowed to stabilize down before the next acceleration, until the set 100rps was reached. Fig. 11 shows the installation of the triaxially orthogonal coils in the test.

The coils responded to the hi-speed rotation of the table, and Fig. 11 gives the induced voltages of the coils. Axis z ran in parallel with the table rotary axle, in this rotation process the coil's effective projection cross area was less than the coil cross area, so axis z produced an induced voltage with a minimal peak.

The data were acquired by the acquisition module of the rotary table and for each coil the sampling rate was 100kHz.

FIGURE 11. Single-axle rotary table layout of triaxially orthogonal coils.

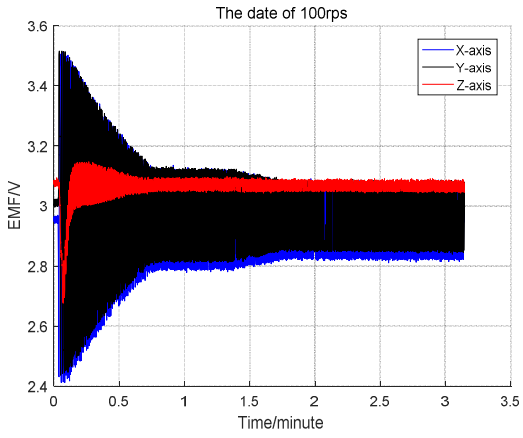

FIGURE 12. Sensor's induced voltage when the single-axle rotary table rate was 100rps.

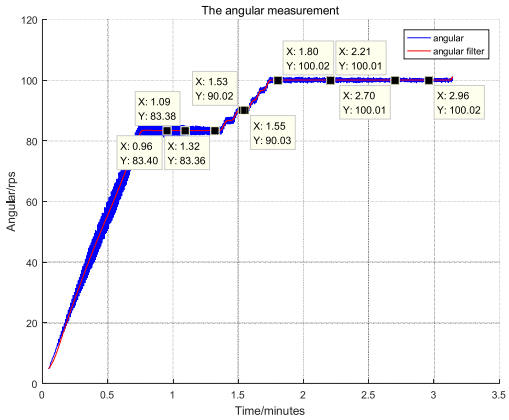

FIGURE 13. Instantaneous single-axle angular speed output by magnetic sensor electronic solver module.

Upon the end of the test, analysis was performed using Eq. (7), the results being shown in Fig. 13. The triaxially orthogonal coils angular rate solver module found that the mean angular rate given by the coils was 100rps when the rotary table became stabilized. The blue curve in Fig. 13

represents the solution given by Eq. (7) whilst the red one represents the ultimate angular rate when low-pass filtering is applied to the solution.

D. ANALYSIS OF TEST RESULTS

The proposed measurement method was demonstrated at a low angular rate of 1r/s in the low rotational speed simulation. According to the simulation results, this measurement system comes with a measurement error of 0.18%FS when measuring a 1r/s rotational speed.

In the medium rotational speed simulation, we checked the measurement system at an angular rate of 40r/s. The simulation results suggest that this measurement system registers a measurement error of 0.175%FS when measuring a 40r/s rotational speed.

In the high rotational speed simulation, we checked the measurement system at an angular rate of 100r/s. The simulation results indicate that the measurement error is 0.02%FS when this system measures a 100r/s rotational speed.

The three simulations suggest that the proposed system adapts not quite well at the initial rotation stage, primarily because the magnetic signal interference and the motion stability are both weak when the simulation installation has just started, resulting in unsteady magnetic induction signal and unsteady output of the minimum detectable angular rate. Similar results were observed nearing the end of rotation.

Because of the unsteadiness during the initial simulation rotation stage, the data acquired at the start or end stages are tainted by drift due to greater magnetic field interference and are therefore rejected. The above tests demonstrate that the proposed sensor is capable of measuring angular rate of low- and high-speed rotation bodies as well as outputting the rotation zero point of the physical quantity.

VII. CONCLUSIONS

A new angular rate measurement method is proposed that makes use of triaxially orthogonal coils to meet the industrial needs for wide-range measurement of rotational angular rate. An analysis is provided that covers the feedback of induced EMF in response to rotational movement. The structure of coils is designed for the magnetic induction angular rate sensor and a model is developed to describe the induced EMF output of the triaxially orthogonal coils in rotary movement. Induced signal zero phase is determined using dual-threshold technique, and the angular rate of a rotational body is evaluated on the basis of zero phase periodicity. From this a method is then proposed that relies on the induced EMF of triaxially orthogonal coils to determine the angular rate in a highly dynamic process. A simulation test involving a hi-precision rotary table operating at 1–100r/s was performed, and the rate as measured was different from the set rate of the table, generating an error within 2‰ FS. The simulation results are found in general agreement with the set values, substantiating the validity of this theoretical model. They also support that the proposed triaxially orthogonal coils can be used to measure 1-100r/s angular rates and can be implemented in engineering application.

REFERENCES

[1] Y.-L. Lu, Y.-J. Pan, L. L. Li, Y. Liu, and H. Peng, "Measurement method of projectile's heading and pitching angle velocities based on biaxial accelerometer," *J. Chin. Inertial Technol.*, vol. 23, no. 2, pp. 160–164, Apr. 2015.

[2] X. He, X. Wang, and D. Li, "Drift trace measurements of ellipsoid rotor axial mass unbalances," *J. Tsinghua Univ.*, vol. 55, no. 3, pp. 322–326, Mar. 2015.

[3] P. Williams, A. Hyslop, M. Stelzer, and M. Kruijff, "YES2 optimal trajectories in presence of eccentricity and aerodynamic drag," *Acta Astronautica*, vol. 64, pp. 745–769, Jan. 2009.

[4] F. Sun and W. Sun, "Research on auto-compensation by rotation in strapdown inertial navigation systems," *Syst. Eng. Electron.*, vol. 23, no. 1, pp. 122–125, Jan. 2010.

[5] Y.-F. Xu, K. Li, G.-L. Yang, and M.-K. He, "Error modeling and compensation for rotation-modulation strapdown inertial navigation system," *J. Comput. Theor. Nanosci.*, vol. 5, no. 2, pp. 981–985, Feb. 2012.

[6] J.-H. Tang, Z.-X. Fu, and Z.-L. Deng, "Identification method for RLG random errors based on allan variance and equivalent theorem," *Chin. J. Aeronautics*, vol. 22, no. 3, pp. 273–278, 2009.

[7] D. Leandro, V. de Miguel-Soto, and M. López-Amo, "High-resolution sensor system using a random distributed feedback fiber laser," *J. Lightw. Technol.*, vol. 34, no. 19, pp. 4596–4602, Oct. 1, 2016.

[8] K.-S. Jiang *et al.*, "A simple and reliable sensor for accurate measurement of angular speed for low speed rotating machinery," *Rev. Sci. Instrum.*, vol. 85, no. 1, p. 015101, Feb. 2014.

[9] N. Chen, C. Tucker, J. M. Engel, Y. Yang, S. Pandya, and C. Liu, "Design and characterization of artificial haircell sensor for flow sensing with ultrahigh velocity and angular sensitivity," *J. Microelectromech. Syst.*, vol. 16, no. 5, pp. 999–1014, Oct. 2007.

[10] L. Wang, Y. Yan, Y. Hu, and X. Qian, "Rotational speed measurement using single and dual electrostatic sensors," *IEEE Sensors J.*, vol. 15, no. 3, pp. 1784–1793, Mar. 2015.

[11] F. G. Jacobitz, K. Schneider, W. J. T. Bos, and M. Farge, "Structure of sheared and rotating turbulence: Multiscale statistics of Lagrangian and Eulerian accelerations and passive scalar dynamics," *Phys. Rev. E, Stat. Phys. Plasmas Fluids Relat. Interdiscip. Top.*, vol. 93, p. 013113, Jan. 2016.

[12] S.-A. Zotov, A.-A. Trusov, and A.-M. Shkel, "High-range angular rate sensor based on mechanical frequency modulation," *J. Microelectromech. Syst.*, vol. 21, no. 2, pp. 398–405, Apr. 2012.

[13] X. Li, J.-J. Qi, Q. Zhang, and Y. Zhang, "Bias-tunable dual-mode ultraviolet photodetectors for photoelectric tachometer," *Appl. Phys. Lett.*, vol. 104, no. 4, p. 041108-4, Jan. 2014.

[14] H.-F. Liu and W.-T. Pike, "A micromachined angular-acceleration sensor for geophysical applications," *Appl. Phys. Lett.*, vol. 109, no. 17, p. 173506, Oct. 2016.

[15] S. E. Alper, Y. Temiz, and T. Akin, "A compact angular rate sensor system using a fully decoupled silicon-on-glass MEMS gyroscope," *J. Microelectromech. Syst.*, vol. 17, no. 6, pp. 1418–1429, Dec. 2008.

[16] P.-D. Pinnoji and J. Nayak, "Design and analysis of a dual-axis resonator fiber-optic gyroscope employing a single source," *Appl. Opt.*, vol. 52, no. 2, pp. 5350–5354, Aug. 2013.

[17] C. Giebeler, D.-J. Adelerhof, A.-E.-T. Kuiper, J.-B.-A. van Zon, D. Oelgeschläger, and G. Schulz, "Robust GMR sensors for angle detection and rotation speed sensing," *Sens. Actuators A Phys.*, vol. 91, no. 1, pp. 16–20, Jun. 2001.

[18] Y.-S. Didosyan, H. Hauser, H. Wolfmayr, J. Nicolics, and P. Fulmek, "Magneto-optical rotational speed sensor," *Sens. Actuators A Phys.*, vol. 106, nos. 1–3, pp. 168–171, 2003.

[19] R. Munguía, "A GPS-aided inertial navigation system in direct configuration," *J. Appl. Res. Technol.*, vol. 12, no. 4, pp. 803–814, 2014.

[20] Y.-W. Guan, S.-Q. Gao, H.-P. Liu, and S.-H. Niu, "Acceleration sensitivity of tuning fork gyroscopes: Theoretical model, simulation and experimental verification," *Microsyst. Technol.*, vol. 21, no. 6, pp. 1313–1323, Jun. 2014.

[21] H. Ghanbarpour, "A back-propagation approach to compensate velocity and position errors in an integrated inertial/celestial navigation system using unscented Kalman filter," *Proc. Inst. Mech. Eng. Part G, J. Aerosp. Eng.*, vol. 228, no. 10, pp. 1702–1712, Jun. 2014.

[22] X.-L. Ning, P.-P. Huang, and J.-C. Fang, "A new celestial navigation method for spacecraft on a gravity assist trajectory," *Math. Problems Eng.*, vol. 2013, no. 1, pp. 927–940, May 2013.

[23] J. Lisa *et al.*, "Recent developments of magnetoresistive sensors for industrial applications," *Sensors*, vol. 15, no. 11, pp. 28665–28689, 2015.

[24] D. Ettelt, P. Rey, G. Jourdan, A. Walther, P. Robert, and J. Delamare, "3D magnetic field sensor concept for use in inertial measurement units (IMUs)," *J. Microelectromech. Syst.*, vol. 23, no. 2, pp. 324–333, Apr. 2014.
[25] K. Li, Y. Han, and R. Yang, "Design of adaptive phase measurement system for variable-frequency signal," *J. North Univ. China (Natural Sci. Edition)*, vol. 37, no. 5, pp. 506–510, 2016.
[26] B.-Q. Du, Y.-F. Wang, W. Zhou, and S.-T. Guo, "High-precision time and frequency measurement method combining time-space conversion and different frequency phase detection," *Sci. China Phys., Mech. Astron.*, vol. 56, no. 11, pp. 2110–2115, Nov. 2013.

KAI LI received the M.Sc. degree from the North University of China, China, in 2008, where he is currently pursuing the Ph.D. degree in signal and information processing. He is also a Lecturer of Signal and Information Processing. His current research interests include electromagnetics and sensor.

Since 2010, he has been involved in magnetic sensor design on integrated transceivers. He holds two patents.

YUAN LI received the Ph.D. degree from the North University of China, China, in 2014. She is currently a Lecturer of Signal and Information Processing.

Her main research interests include signal and information processing, optical device, and sensor.

Since 2009, she has been involved in sensor design, and various active and passive devices in advanced IC processes. She holds one patent.

YAN HAN received the Ph.D. degree from the Beijing Instituute of Technology, China, in 1998.

He is currently a Professor of Signal and Information Processing, where he has been a Ph.D. Supervisor and the Director of the Research Center in Computer Aided Electrical Engineering since 1998.

His main research interests include signal and information processing, destructive detection, and sensor.